Hurst's Analysis to Detect Minimum Fluidization and Gas Maldistribution in Fluidized Beds

C. L. Briens, L. A. Briens, J. Hay, C. Hudson, and A. Margaritis
Dept. of Chemical and Biochemical Engineering, University of Western Ontario, London, Ontario, Canada, N6A 5B9

Gas-liquid-solid fluidized beds are used extensively in the refining, petrochemical, pharmaceutical, biotechnology, food, and environmental industries. An extensive review of gas-liquid-solid fluidization has been published by Fan (1989).

The performance of multiphase reactors is affected by the flow regime and the quality of the gas distribution. The liquid and gas velocities at which flow regime transitions occur depend on liquid and solid properties which often evolve unpredictably in industrial reactors (Nacef et al., 1991; Wild et al., 1984). There is at present no reliable method to identify the flow regime in industrial gas-liquid-solid fluidized beds. Even well-designed reactors encounter gas distribution problems as the distributor becomes plugged or particles agglomerate and form defluidized zones.

Simple, robust and effective ways of determining the flow regime and the gas distribution in industrial units would make it possible to maintain optimal operating conditions through on-line control of liquid or gas velocity. The various measurement systems may be classified according to the scale of their measuring volume. First, probes such as bubble probes have a measurement volume smaller than the size of most bubbles and particles (Saxena et al., 1988). Second, "local probes" have a measurement volume smaller than the reactor cross-section. Third, cross-sectional probes measure cross-sectional averages. Fourth, bed average probes measure at the scale of the bed volume. All these probes measure properties such as capacitance, conductivity, density, light, or γ-ray absorption (Deckwer, 1992; Fan, 1989; Hetsroni, 1982). Their application to on-line control of industrial units is impaired by their sensitivity to fouling, misalignment, and variations in particle or liquid properties.

Although nonlinear chaos analysis of a probe signal can provide useful information, it is time-consuming and requires an expert for the selection of parameters such as delay time (Hay et al., 1996). This makes it unsuitable for on-line process-control.

Hurst's rescaled range analysis of a probe signal is not significantly affected by moderate changes in probe calibration constants (Hurst, 1951). Hurst's analysis of probe signals could eliminate problems associated with changes in probe, liquid, or solid characteristics. Its simplicity and rapidity make it suitable for on-line process control.

Hurst exponents were obtained from pressure signals in gas-liquid-solid fluidized beds by Fan et al. (1990) who did not relate them to hydrodynamics and by Kwon et al. (1994) who did. Fan et al. (1993) attributed variations in Hurst exponent from pressure signals in a liquid-solid fluidized bed to changes in solid mixing. Latifi et al. (1994) applied Hurst's analysis to the local liquid-solid mass-transfer fluctuations in a trickle bed. Drahos et al. (1992) used Hurst's analysis to discriminate between flow regimes in a gas-liquid bubble column. Franca et al. (1991) similarly identified flow regimes in horizontal gas-liquid pipe flow. Hurst's analysis has been applied to many other natural phenomena (Feder, 1988).

The objective of this article is to establish whether the hydrodynamics of gas-liquid-solid fluidized beds can be characterized through Hurst's analysis of signals obtained from a variety of probes. Two problems of industrial importance for fluidized beds are focused on: the detection of gas maldistribution and the identification of fluidization regimes.

Equipment and Experimental Methods

Two fluidization columns were used in this study: an 8-cm-dia. column for the gas maldistribution experiments and a 10-cm-dia. column for the fluidization regimes study. The liquid was an aqueous solution of 1 wt. % of $NaHPO_4$, the gas was oil-free air and the particles were 3 mm spherical, monosize glass beads with a density of 2,470 kg/m^3.

In all cases, the probe signal was acquired with a high precision 16 bit card at a frequency of 500 Hz for 60 s, yielding a time series of 30,000 points. No frequency filter was applied to the signal. Spectral analysis failed to identify any dominant frequency.

- The bubble probe was made of two 0.5-mm stainless steel needles spaced 1 mm apart to which an alternating sinusoidal potential of 5 V and 2,500 Hz was applied (this alternating potential was also used for the conductivity probes). Even very small bubbles, which did not span the gap between the needles, yielded a detectable change in the signal.
- Local probes consisted of two solid stainless steel rods, 4.8 mm in diameter which were coated with insulating Rilsan

Correspondence concerning this article should be addressed to C. L. Briens.

except for the tips for a 9 mm electrode length. The two tips were placed at a vertical distance of 5 cm apart and at the same radial position.

- The cross-sectional conductivity probe consisted of two radially opposed wall electrodes, 30 cm above the grid, made of 1 cm × 6 cm platinized titanium mesh.
- The bed-average conductivity probe consisted of two radially opposed wall electrodes, one located 10 cm and the other 50.5 cm above the grid.
- The bed-average pressure gradient was obtained with a fast-response (< 1 ms) differential transducer. The two wall pressure taps were 6 cm and 46 cm above the grid.
- The pressure difference across the bed surface was also obtained with an identical pressure transducer. The first tap was 51 cm and the second was 71 cm above the grid.

Calculations for Hurst's Rescaled Range Analysis

Hurst invented a new method of analysis for the time series of natural phenomena (Hurst, 1951). Hurst worked with time as a series set of discrete data. If the steps in the time series are sufficiently small then the time series of discrete points may be described as a function with derivative $y(t)$. The Hurst exponent of this function may be calculated through the following steps: (1) Divide the time series in N intervals of length τ_H, called "subperiods"; (2) for each subperiod k.

(a) Calculate the signal average for this subperiod which starts at time t_k

$$\bar{y}_k = \frac{1}{\tau_H} \int_{t_k}^{t_k + \tau_H} y(t)\, dt \tag{1}$$

(b) Calculate the standard deviation of the signal

$$S_k = \left[\frac{1}{\tau_H} \int_{t_k}^{t_k + \tau_H} (y(t) - \bar{y}_k)^2 \right]^{1/2} \tag{2}$$

(c) Calculate the accumulated departure from the average

$$X(t) = \int_{t_k}^{t_k + t} (y(u) - \bar{y}_k)\, du \tag{3}$$

(d) Calculate the minimum $X_{k,\min}$ and the maximum $X_{k,\max}$ of the accumulated departure values over the subperiod k.

(e) Calculate the range over the subperiod k

$$R_k = X_{k,\max} - X_{k,\min} \tag{4}$$

(f) Calculate the rescaled range for subperiod k

$$(R/S)_k = R_k/S_k \tag{5}$$

(3) Average the $(R/S)_k$ obtained for the N subperiods

$$(R/S)_{\tau_H} = \frac{1}{N} \sum_{k=1}^{N} (R/S)_k \tag{6}$$

Repeating steps 1 through 3 for various values of the subperiod length τ_H, one can obtain the variation of the average rescaled range $(R/S)_{\tau_H}$ with τ_H. The Hurst exponent H is then estimated with the following equation

$$H = \frac{d[\ln (R/S)_{\tau_H}]}{d\,[\ln (\tau_H)]} \tag{7}$$

The Hurst exponent is, thus, the slope of the log-log plot of $(R/S)_{\tau_H}$ against τ_H.

For a random walk process such as Brownian motion, there is no correlation between past and future increments and the Hurst exponent is 0.5. An exponent greater than 0.5 indicates persistence in the data, that is, the trend in the time series, whether increasing or decreasing, will likely continue. An exponent less than 0.5 indicates antipersistence in the data, that is, the trend will likely reverse itself. A detailed mathematical analysis can be found in Feder (1988) and Peters (1994).

Experimental Results and Discussion

High- and low-frequency Hurst exponents

Figure 1 shows that the rescaled range (R/S) for the three-phase systems varied with the subperiod length τ_H in a similar manner for all the measurement methods in log-log coordinates. Similar results were obtained for all the liquid and gas velocities and for all flow regimes. In all cases, the slope was steeper at small subperiod lengths than at large subperiod lengths. There was a smooth transition between these two extreme regions (Figure 1). Since the regions of interest are those where the slope H is constant, the (R/S) values obtained at both ends of the range of subperiod length must be accurate.

To increase the accuracy of the slope H at small subperiod lengths, the rescaled range (R/S) was calculated for all possible subperiod lengths above 20 ms. Each subperiod contained at least ten original data points, as recommended by

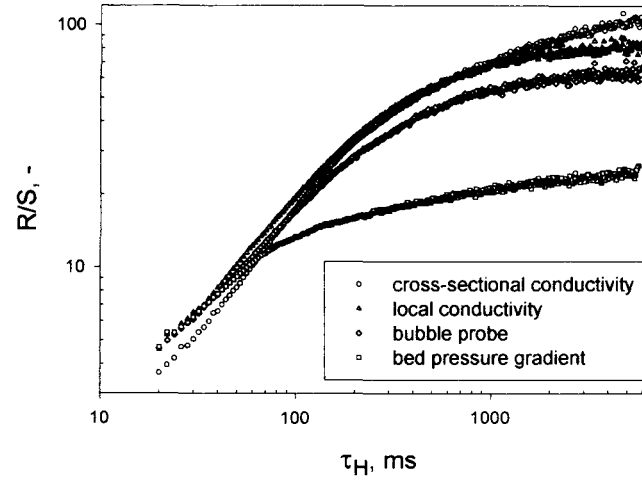

Figure 1. Variation of the rescaled range with the subperiod length for various measurement devices.

V_g = 6 cm/s; V_L = 3 cm/s.

Peters (1994). To get as many (R/S) values as possible, (R/S) was then calculated for all possible subperiod lengths, that is, all multiples of the original data time interval. The resulting increase in computation time was more than justified by the increased accuracy.

To increase the accuracy of the slope H at large subperiod lengths, the record length was first increased to 30,000 points for a total sampling time of 60 s. Figure 1 shows that there was significant scatter at large subperiod lengths, even when using a minimum of ten contiguous subperiods. To determine an accurate exponent, H required increasing the number of (R/S) values at large subperiod lengths τ_H. This cannot be achieved when using subperiod lengths which are exact divisors of the total record length, as recommended by Peters (1994) to ensure that each (R/S) estimate uses all the original data. Korsan (1993) takes a random starting point for each subperiod to increase the number of subperiods. Since subperiods are overlapping, this greatly increases the computation time. The present study takes a simpler approach. The rescaled range is calculated with contiguous subperiods of all possible lengths, even though the subperiod length may not be an exact divisor of the total record length. Since each record contains 30,000 points, the fraction of the points which may be dropped at the end of the record is small (such as for subperiods ranging to 6,000 ms, the maximum number of dropped points was 48 which is 0.16% of the total record).

The Hurst exponents shown in Figure 2 were obtained from Figure 1 by applying a smoothing spline to each curve and taking its derivative. Two regions appear at both ends of the subperiod length scale and are connected by a smooth transition region. The "high frequency Hurst exponent" is obtained for subperiod lengths of 20 to 60 ms, that is, for frequencies of 15 to 50 Hz. The "low frequency Hurst exponent" is obtained for subperiod lengths of 2,000 to 6,000 ms, that is, for frequencies of 0.15 to 0.5 Hz. The analysis presented herein and the development of the low frequency Hurst exponent depends on having a large record length, such as the 30,000 points used in this study.

In all cases, the low frequency Hurst exponent was well below 0.5, indicating an antipersistent system behavior, that

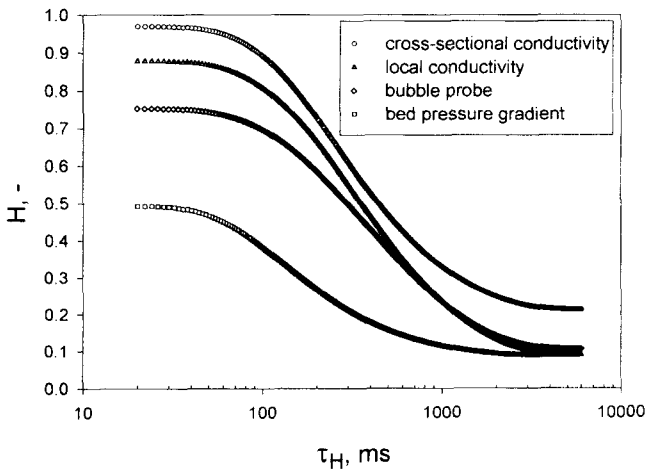

Figure 2. Variation of the Hurst exponent with the subperiod length for various measurement devices.

$V_g = 6$ cm/s; $V_L = 3$ cm/s.

is, the trend will likely reverse itself (Figure 2). A possible explanation is that from time to time at random intervals several medium-sized gas bubbles rising through the bed coalesce, forming a very large bubble. Such a large bubble will be detected by all the measurement probes used in this study. The very large bubble rises quickly though the bed sweeping the medium-sized bubbles which could have coalesced into another very large bubble. Another very large bubble is thus unlikely to occur right away, giving an antipersistent signal.

The high frequency Hurst exponent of the bubble probe signal was about 0.75 (Figure 2). It is persistent indicating that the gas flow triggering the signal comes in groups. This suggests that gas flows in trains or "chains" of smaller bubbles, some of which may be caught in local circulation patterns.

As the probe measurement volume is increased, the high frequency Hurst exponent becomes larger, indicating more persistent behavior (Figure 2). At any given time, a cross-sectional probe is more likely to continue detecting bubbles than a bubble probe whose detection volume is much smaller. The detection volumes of both probes are still small enough to be affected by individual bubbles and, thus, they detect persistence.

On the other hand, no persistence is detected with the bed pressure gradient, since the high frequency Hurst exponent is only about 0.5, which is the Hurst exponent of a random, Brownian motion. The pressure transducers detect fluctuations occurring over the whole column. Their detection volume includes a large number of smaller bubbles whose global behavior appears random. However, the large bubbles are still relatively infrequent and can be individually detected even at this scale. This explains why their antipersistent behavior can be identified from the pressure gradient which yields a low frequency Hurst exponent of less than 0.5.

Detection of gas maldistribution

The radial profile of the gas holdup in a gas-liquid-solid fluidized bed was obtained from a bubble probe, positioned 30 cm from the grid at nine radial locations using an intricate calibration procedure (Hudson, 1996). When the column was vertical, there was more gas at the center than near the wall, which indicates that the gas distributor was operating properly (Hudson, 1996).

The high frequency Hurst exponent gives a similar radial profile (Figure 3). The Hurst exponent was obtained directly from a local conductivity probe signal, without any calibration. Figure 3 shows that the signal was persistent in the center and antipersistent near the wall. (R is the inside column diameter and r is the radial coordinate ($r = 0$ at center; in the inclined column, $r < 0$ for the low column wall side.)) Since the local probe is affected primarily by relatively large bubbles, the flow of such bubbles was regular at the center and irregular near the wall. For a large bubble to form by coalescence near the wall, enough bubbles had to be accumulated there by eddies or wall effects. The large bubble then swept smaller bubbles from this region, preventing the immediate formation of another large bubble.

The maximum of the V statistic over the whole subperiod range also gave a similar radial profile (Figure 3). The V statistic was proposed by Hurst (1951) and successfully used

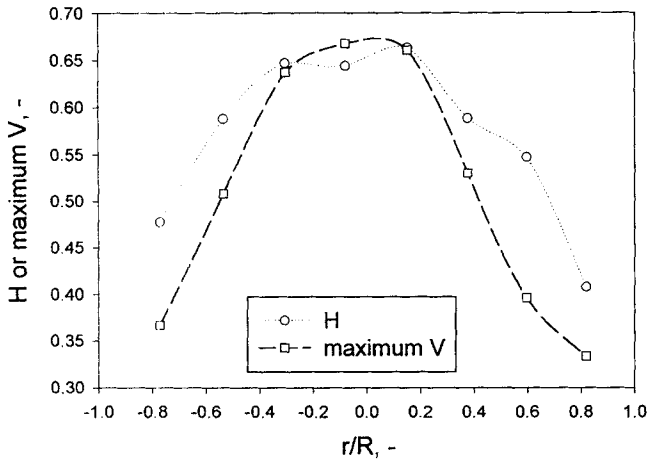

Figure 3. Application of Hurst's analysis to the local conductivity in the vertical column: radial profiles of high frequency Hurst exponent and maximum V value.

$V_g = 12$ cm/s; $V_L = 6.8$ cm/s.

by Peters (1994) to measure the strength of the cyclic nonperiodic behavior of a time series. It has never been used for chemical engineering applications. It is defined as

$$V_{\tau_H} = \frac{(R/S)_{\tau_H}}{\sqrt{\tau_H}} \tag{8}$$

Inclining the column by 10° led to a strong gas maldistribution, as shown in Figure 4 (Hudson, 1996). This gas maldistribution can be detected from the high frequency Hurst exponent (Figure 4). The occurrence of large bubbles was antipersistent everywhere. The large bubble flow was not as regular as in the vertical column, even in the region of maximum gas holdup. Since little gas flows parallel to the liquid flow in the inclined column, the gas flow is antipersistent. The maximum of the V statistic amplifies the regions of high gas holdup and provides an even better detection of the gas maldistribution (Figure 4). Similar results were obtained under other conditions.

Hurst analysis can therefore be used to identify regions of high gas holdup in gas-liquid-solid fluidized beds. Instead of using a fragile and easily fouled bubble probe which requires an intricate calibration, one can use a much more sturdy local probe without any calibration.

Determination of the fluidization regime

All the results presented in this section were obtained at a superficial gas velocity of 6 cm/s in the 10-cm-dia. column. Similar results were obtained with gas velocities ranging from 3 to 12 cm/s.

Visual observations identified three distinct fluidization regimes as the superficial liquid velocity was decreased from 5.6 to 0.4 cm/s. At high velocities, the fluidization was uniform, with vigorous and smooth solids backmixing. When the velocity was decreased below about 2 cm/s, solids backmixing occurred slowly in spurts and the bed started compacting. The effect of the gas bubbles appeared similar to that of a mechanical vibrator; this regime was called "agitated." As the liquid velocity was decreased below about 1 cm/s, the bed became completely fixed.

None of the standard time-averaged probe signals provided clear-cut detection of both visually observed regime transitions. The fluctuations of the same signals were therefore analyzed to obtain their Hurst exponents. In all cases, the equations of the straight lines and the velocities at which they intersect were determined by minimizing the sum of squared differences between the Hurst exponents obtained from Hurst's analysis and the values predicted from the straight lines. This ensured an objective determination of the transition velocities. For example, Figure 5 shows that the low frequency Hurst exponent from the local conductivity meaurements identifies the two regime transitions. (V_L is superficial liquid velocity, m/s; V_g is the superficial gas velocity, m/s).

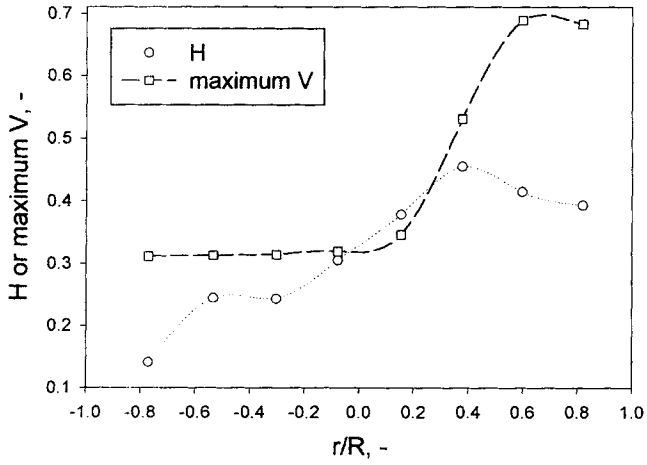

Figure 4. Application of Hurst's analysis to the local conductivity in a 10° inclined column: radial profiles of high frequency Hurst exponent and maximum V value.

$V_g = 12$ cm/s; $V_L = 6.8$ cm/s.

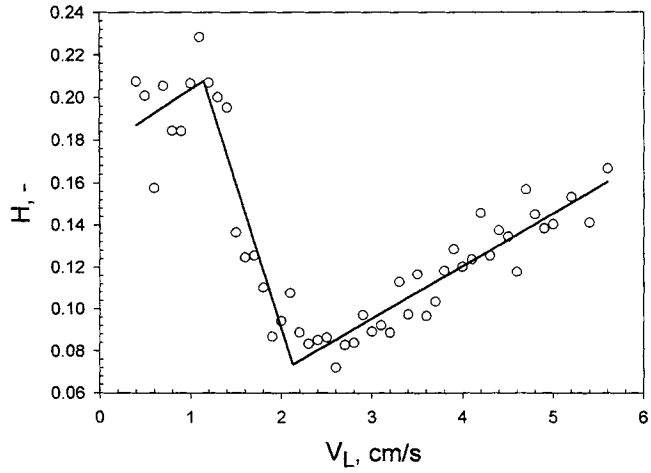

Figure 5. Variation with the superficial liquid velocity of the low frequency Hurst exponent obtained from the local conductivity.

$V_g = 6$ cm/s.

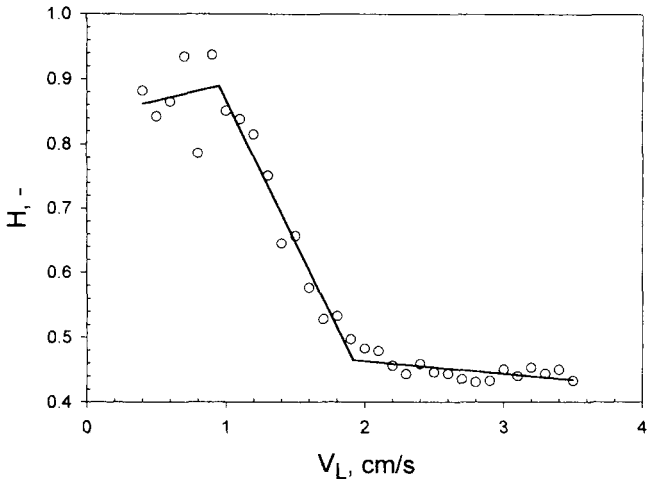

Figure 6. Variation with the superficial liquid velocity of the high frequency Hurst exponent obtained from the pressure drop across the bed surface

V_g = 6 cm/s.

The transition from the agitated to fixed-bed flow regime could be clearly identified from the variation with liquid velocity of the high frequency Hurst exponent obtained from either the cross-sectional average or local conductivity signals. It could also be identified from the variation of the low frequency Hurst exponent from the bed average conductivity.

The transition from the fluidized to agitated flow regime could be clearly identified from the variation with liquid velocity of the high frequency Hurst exponent obtained from either the bed average, cross-sectional average, or local conductivity signals. It could also be identified in the same manner from the bubble probe signals.

In many industrial applications, however, the main objective is to determine whether a bed is fluidized and varying the liquid velocity over a wide range to determine the minimum fluidization velocity would be awkward. The pressure drop across the bed surface therefore seems to be most practical for industrial control: if its high frequency Hurst exponent is kept below a critical value, the bed is fluidized (Figure 6).

Conclusions

The hydrodynamics of gas-liquid-solid fluidized beds can be characterized through Hurst's analysis of signals obtained from a variety of measurement probes. Since Hurst's analysis characterizes the structure of the probe signals, it can tolerate changes in probe calibration constants.

Gas maldistribution can be detected from the radial profile of Hurst exponents obtained from such measuring devices as sturdy local conductivity probes. Hurst's analysis will, thus, allow the simple detection of gas maldistribution in environments unsuitable for delicate bubble probes.

Hurst's analysis provides clear identification of the fluidization regime transitions from a variety of measurement devices, ranging in scale from bubble probes to bed average conductivity and pressure measurements. While none of the time-averaged signals obtained from the six different measurement devices used in this study could identify the fixed to agitated bed and the agitated to fluidized transitions, Hurst's analysis successfully detected these two transitions from any single measurement probe. Results such as those obtained with the pressure drop across the bed surface are most practical for industrial control: if the high frequency Hurst exponent is kept below a critical value, the bed is fluidized.

Acknowledgments

The authors gratefully acknowledge the financial support from the Natural Sciences and Engineering Research Council (NSERC) of Canada, in the form of an Operating Research Grant to C. L. Briens and Scholarships to L. A. Briens and C. Hudson. The authors also wish to thank V. P. Briens for keeping to bare facts.

Literature Cited

Deckwer, W. D., *Bubble Column Reactors*, Wiley, New York (1992).

Drahos, J., F. Bradka, and M. Puncochar, "Fractal Behavior of Pressure Fluctuations in a Bubble Column," *Chem. Eng. Sci.*, **47**, 4069 (1992).

Fan, L. S., *Gas-Liquid-Solid Fluidization Engineering*, Butterworths, Boston (1989).

Fan, L. T., D. Neogi, M. Yashima, and R. Nassar, "Stochastic Nature of a Three-Phase Fluidized Bed. Fractal Approach," *AIChE J.*, **36**, 1529 (1990).

Fan, L. T., Y. Kang, D. Neogi, and M. Yashima, "Fractal Analysis of Fluidized Particle Behavior in Liquid-Solid Fluidized Beds," *AIChE J.*, **39**, 513 (1993).

Feder, J., *Fractals*, Plenum Press, New York (1988).

Franca, F., M. Acikgoz, R. T. Lahey, and A. Clausse, "The Use of Fractal Techniques for Flow Regime Identification," *Int. J. Multiphase Flow*, **17**, 545 (1991).

Hay, J., C. Hudson, and C. L. Briens, "Correlation Dimension for a Gas-Liquid Contactor," *Chem. Eng. J.*, **64**, 157 (1996).

Hetstroni, G., *Handbook of Multiphase Systems*, McGraw Hill, New York (1982).

Hudson, C., "Effect of Inclination on Hydrodynamics and Heat Transfer in Bubble Columns, Liquid-Solid and Gas-Liquid-Solid Fluidized Beds," PhD thesis, Univ. of Western Ontario, London, Canada (1996).

Hurst, H. E., "Methods of Using Long-Term Storage in Reservoirs," *Trans. American Soc. of Civil Engineers*, **116**, 770 (1951).

Korsan, R. J., "Fractals and Time Series Analysis," *Mathematica J.*, **3**(1), 39 (1993).

Kwon, H. W., Y. Kang, S. D. Kim, M. Yashima, and L. T. Fan, "Bubble-Chord Length and Pressure Fluctuations in Three-Phase Fluidized Beds," *Ind. Eng. Chem. Res.*, **33**, 1852 (1994).

Latifi, M. A., A. Naderifar, N. Midoux, and A. Le Mehauté, "Fractal Behaviour of Local Liquid-Solid Mass Transfer Fluctuations at the Wall of a Trickle-bed Reactor," *Chem. Eng. Sci.*, **49**, 3823 (1994).

Nacef, S., S. Poncin and G. Wild, "Onset of Fluidisation and Flow Regimes in Gas-Liquid-Solid Fluidisation—Influence of the Coalescence Behaviour of the Liquid," *La Fluidisation*, C. Laguerie and P. Guigon, eds., Lavoisier Technique et Documentation, Paris, 359 (1991).

Peters, E. E., *Applying Chaos Analysis to Investment and Economics*, Wiley, New York (1994).

Saxena, S. C., D. Patel, D. N. Smith, and J. A. Ruether, "An Assessment of Experimental Techniques for the Measurement of Bubble Size in a Bubble Slurry Reactor as Applied to Indirect Coal Liquefaction," *Chem. Eng. Commun.*, **63**, 87 (1988).

Wild, G., M. Saberian-Broudjenni, and J. C. Charpentier, "Gas-Liquid-Solid Fluidized Bed Reactors," *Int. Chem. Eng.*, **24**, 632 (1984).

Manuscript received Apr. 23, 1996, and revision received Feb. 27, 1997.